An Advection Scheme for the Transport of Fractional Volume of an Incompressible Fluid

Ho Sang Kwak*[1] and Kunio Kuwahara*[2]

비압축성 유체의 체적비 수송에 대한 대류항 계산 기법

곽호상, Kunio Kuwahara

서로 섞이지 않는 두 비압축성 유체의 유동을 해석하기 위하여 VOF 방법에 기초한 수치기법을 개발하였다. 유체간의 계면형상의 거동은 유동장내의 유체의 점유체적비의 변화에 의해 묘사되는데 이를 지배하는 이동방정식을 풀기 위한 새로운 대류항 계산법을 고안하였다. 대류항은 유체계면의 방향에 따라 풍상법과 역풍상법의 적절한 조합을 취하여 계산하는데 여기에 대각방향의 상류효과를 포함시켜 시간에 대한 2차 정확도를 갖도록 하였다. 또한 이 방법을 유량보정수송(FCT)법과 결합시켜 해의 단조성을 보장하였다. 몇 가지 단순 문제에 대한 시험 결과 이 기법이 수치오차에 의한 계면형상의 변형과 파손을 감소시킴을 확인하였다.

Key Words: 유체체적비법(Volume of Fluid Method), 유량보정수송(Flux-Corrected Transport), 유체 계면(Interface between two immiscible fluids), 대각방향 상류효과 (Cross-Directional Upstream Effects), 단조성(Monotonicity)

1. Introduction

Several numerical methods [1-6] have been proposed to describe flows of assemblies of immiscible fluids. These flows are characterized by the presence of interface which divides the flow domain into regions of individual component fluids. The interface is identified to be a demarcation surface across which steep changes or discontinuities in fluid properties take place. One overriding concern is that, throughout the flow domain, the constraint of divergence-free as well as mass conservation should be satisfied. These pose considerable difficulties in achieving a robust and efficient numerical solution algorithm.

One widely-utilized technique is the interface tracking method, which is based on the Lagrangian description of interface motion, e.g., the marker-and-cell method [1-2] and the smooth particle hydrodynamics [3]. This approach enjoys the advantages of logical simplicity and easy extension to multi-dimensional problems. The drawbacks are huge storage requirement and difficulties encountered in dealing with topological change of interface and ensuring global constraints of mass and momentum conservations.

Another well-established routine, termed the interface capturing method, calls for one or more additional field variables to identify fluid phase

*[1] 정회원, 시스템공학연구소 슈퍼컴퓨터센터
*[2] Associate Professor, The Institute of Space and Astronautical Science (ISAS), Japan

[4-6]. Among them, the volume of fluid (VOF) method [4], which employs the fractional volume of a fluid in mixture of immiscible fluids, has several advantages, e.g., minimum storage requirement and compatibility with the existing finite volume algorithms. The conservation equation for this variable is solved by using an advection scheme on an arbitrary Lagrangian-Eulerian mesh. The fluid interface is traced by monitoring sharp variations of volume fraction. Disadvantages are that numerical errors are generated by advection scheme, which turn up in the form of unphysical numerical diffusion and dispersion. For a successful application of this method, an accurate advection scheme is essential to capture the discontinuities and to force them to propagate with the proper interface velocity.

Serious efforts have been given to designing an accurate advection scheme suitable for VOF and appreciable improvements have been reported [4-5]. However, the preceding advection schemes are still of low-order of accuracy both in time and space. Furthermore, the basic framework is grounded on uni-directional consideration for convection terms. Consequently, a relatively accurate prediction is possible for one-dimensional interface propagation; however, for multi-dimensional problems, these methods produce undesirable numerical deformations. Additional defect is that the prior advection schemes [4-5] do not yield monotone solution. Local overshoots and undershoots can be included in the solution. As a remedy, an explicit cut-off was often effectuated to limit the volume fraction within certain range.

The primary aim of the present study is to design a new advection scheme which addresses these shortcomings of the existing methods based on the VOF approach.

2. Basic Model of VOF

Consider a flow of two immiscible fluids, fluid 1 and fluid 2, of different densities ρ_1 and ρ_2, respectively. The VOF technique introduces an additional field variable, C, the volume fraction of fluid 1, such that C=1 inside the region of fluid 1 and C=0 in the region of fluid 2. The density in the domain is given by

$$\rho = \rho_1 C + \rho_2 (1 - C). \tag{1}$$

In this study, method derivation is made for a two-dimensional flow configuration. The equation of mass conservation, together with the constraints of incompressibility of both fluids enforces the divergence-free velocity field and the transport equation for C:

$$\frac{\partial u}{\partial x} + \frac{\partial v}{\partial y} = 0, \tag{2}$$

$$\frac{\partial C}{\partial t} + \frac{\partial (uC)}{\partial x} + \frac{\partial (vC)}{\partial y} = 0, \tag{3}$$

where t is the time, x and y are the horizontal and vertical coordinates, respectively. (u, v) is the velocity vector in the (x,y) domain.

A finite-volume formulation is conducted on a staggered grid system as shown in Fig. 1. Integration of Eq. (3) over a control volume (width Δx_i and height Δy_j) and over a time interval Δt yields a discretized equation:

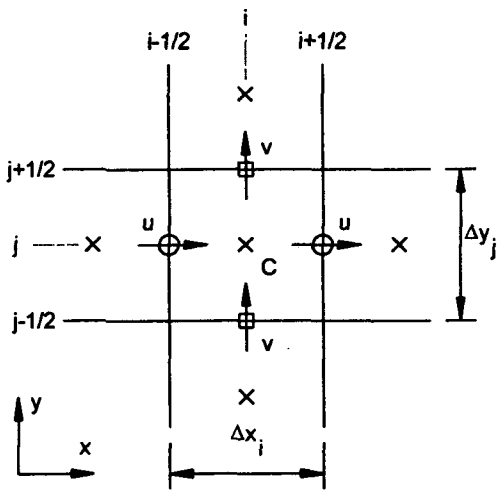

Fig. 1 Finite volume grid configuration.

$$(C_{i,j}^{n+1}-C_{i,j}^{n})V_{i,j}$$
$$=f_{i-1/2,j}-f_{i+1/2,j}+f_{i,j-1/2}-f_{i,j+1/2}, \quad (4)$$

where f is flux of C at the cell boundaries and $V_{i,j}$ is the volume of the cell.

A standard method to estimate f is the upwind method. The upwind flux in the horizontal direction, $f_{i-1/2,j}^{u}$, based on donor (upstream-side) cell concept, is given by

$$f_{i-1/2,j}^{u}=\begin{cases} Q_{i-1/2,j}C_{i-1,j}^{n} & \text{for } Q_{i-1/2,j}\geq 0 \\ Q_{i-1/2,j}C_{i,j}^{n} & \text{for } Q_{i-1/2,j}<0, \end{cases} \quad (5)$$

where $Q_{i-1/2,j}$ is the volume flux defined as $Q_{i-1/2,j}=u_{i-1/2,j}\Delta y_j\Delta t$. This flux can be, in a more general form, expressed as

$$f_{i-1/2,j}^{u}=Q_{i-1/2,j}C_{i-1/2-p/2,j}^{n}, \quad (6a)$$

where $p=sign(Q_{i-1/2,j})$. Similarly, the upwind flux in the vertical direction, $f_{i,j-1/2}^{u}$, becomes

$$f_{i,j-1/2}^{u}=Q_{i,j-1/2}C_{i,j-1/2-q/2}^{n}, \quad (6b)$$

where $Q_{i,j-1/2}=v_{i,j-1/2}\Delta x_i\Delta t$ and $q=sign(Q_{i,j-1/2})$.

In contrast, the downwind fluxing scheme uses the value in the acceptor (downstream-side) cell. In an analogous manner to Eq. (6), the downwind fluxes, $f_{i-1/2,j}^{d}$ and $f_{i,j-1/2}^{d}$, are defined as

$$f_{i-1/2,j}^{d}=Q_{i-1/2,j}C_{i-1/2+p/2,j}^{n}, \quad (7a)$$
$$f_{i,j-1/2}^{d}=Q_{i,j-1/2}C_{i,j-1/2+q/2}^{n}. \quad (7b)$$

Obviously, in these fluxing schemes, only the nearest neighboring grid points are taken into consideration. The upwind (downwind) scheme portrays correctly the interface speed when interface is nearly parallel (perpendicular) to flow. The drawback of the upwind scheme is the numerical diffusion which tends to smear out interface over a number of grid points. The downwind scheme enjoys a favorable capability of surface sharpening but is prone to numerical instability [5].

In this study, two fluxing operators are introduced for a brief description:

$$Fx(a,j,Q,C,V,\theta)$$
$$=\begin{cases} QC_{a-s/2,j} & \text{for } \theta_{a-s/2,j}^{x}\geq\theta^{c} \\ s\cdot\max[\ \widetilde{Fx}_{a,j}, Gx_{a,j}] & \text{for } \theta_{a-s/2,j}^{x}<\theta^{c}, \end{cases} \quad (8a)$$

$$Fy(i,a,Q,C,V,\theta)$$
$$=\begin{cases} QC_{i,a-s/2} & \text{for } \theta_{i,a-s/2}^{y}\geq\theta^{c} \\ s\cdot\max[\ \widetilde{Fy}_{i,a}, Gy_{i,a}] & \text{for } \theta_{i,a-s/2}^{y}<\theta^{c}, \end{cases} \quad (8b)$$

where

$$\widetilde{Fx}_{a,j}=\min[\,QC_{a+s/2,j}, C_{a-s/2,j}V_{a-s/2,j}],$$
$$Gx_{a,j}=|Q|-(1-C_{a-s/2,j})V_{a-s/2,j},$$
$$\widetilde{Fy}_{i,a}=\min[\,QC_{i,a+s/2}, C_{i,a-s/2}V_{i,a-s/2}],$$
$$Gy_{i,a}=|Q|-(1-C_{i,a-s/2})V_{i,a-s/2},$$

in which $s=sign(Q)$.

In an effort to rectify the above-described disadvantages, Lafaurie et al. [5] devised a fluxing scheme based on a weighted average of these two fluxes. The scheme of Lafaurie et al. [5] can be represented as

$$f_{i-1/2,j}=Fx(i-1/2,j,Q_{i-1/2,j},C,V,\theta), \quad (9a)$$
$$f_{i,j-1/2}=Fy(i,j-1/2,Q_{i,j-1/2},C,V,\theta). \quad (9b)$$

The idea is to select a proper fluxing scheme in light of the relative orientation of interface. The downwind (upwind) scheme is selected when the interface is mainly perpendicular (parallel) to the flow direction. To this end, the directional angles of interface are calculated

$$\theta^{x}=\cos^{-1}(|n^{x}|), \quad (10a)$$
$$\theta^{y}=\cos^{-1}(|n^{y}|), \quad (10b)$$

where n^{x} and n^{y} are the x- and y-components of unit normal vector to interface, $\mathbf{n}=\nabla C/|\nabla C|$, as

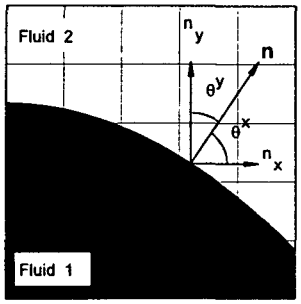

Fig. 2 Directional angle of interface.

shown in Fig. 2. The optimal values of θ^c in Eq. (8) were suggested $1.0<\theta^c<1.05$ [5].

3. Fluxing Scheme Including the Cross-Directional Upstream Effects

The scheme of Eq. (9), which provides an accurate prediction of interface motion in one-dimensional flow, can create undesirable numerical errors under multi-dimensional situations. Fig. 3 is illustrative of such interface deformation. A two-dimensional square domain filled with fluid 1 is propagated in a uniform flow field $(u,v)=(1,1)$ during a unit time step. As seen in Fig. 3(b), the cell A can not feel any impact of the upstream cell B, since all the fluxes advected into cell A do not contain any information of cell B. Consequently, the region near leading edge undergoes distortions. In a similar manner, shape changes can take place mainly in the corner regions as shown in Fig. 3(a). Another type of numerical interface deformation may be found when a rectangular domain is rotated (see, e.g. [5]). Numerical errors turn up in the form of large amounts of flotsam on large lattice and spatial zigzag oscillations on the surfaces.

These anomalies are due to the one-dimensional-like representation of flux terms. One significant approach to minimize these errors is

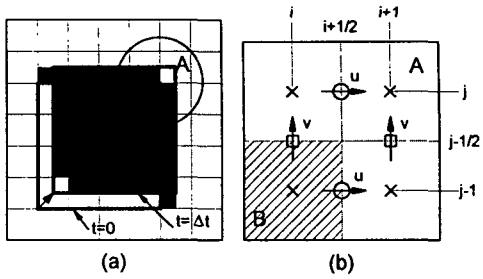

Fig. 3 Pure propagation of a square domain in a uniform velocity field $(u,v)=(1,1)$. The heavy lines indicate the initial condition (t=0) and the exact solution after a time step, $\Delta t=0.5\Delta x/u$. The shaded area in frame (a) represents the numerical solution acquired by Eq.(9). Fig. 3(b) shows an enlarged view near the leading edge of the square at t=0.

to include the cross-directional stream effects. Fig. 4 portrays the baseline idea to do this.

Consider a vertical transport of C from the cell $(i,j-1)$ to the cell (i,j) by $Q_{i,j-1/2}(>0)$. The volume occupied by fluid 1 in the cell (i,j) at $t=t_n$ is represented by the area of region (A+B) in Fig. 4. Allowing a strictly one-dimensional transport due to $Q_{i,j-1/2}$, the volume of fluid 1 in the cell (i,j) at time $t=t_{n+1}$ becomes the area of the region (B+C). Thus, a second-order approximation of C in the cell (i,j) at time $n+1/2$ can be estimated as

$$C_{i,j}^{n+1/2} \approx \frac{C^{A+B}+C^{B+C}}{2} = \frac{C_{i,j}+C^{B+C}}{2}. \quad (11)$$

The area of region C is equivalent to the amount of volume fraction advected into the cell (i,j) from the lower cell $(i,j-1)$ during Δt via $Q_{i,j-1/2}$. This can be estimated as

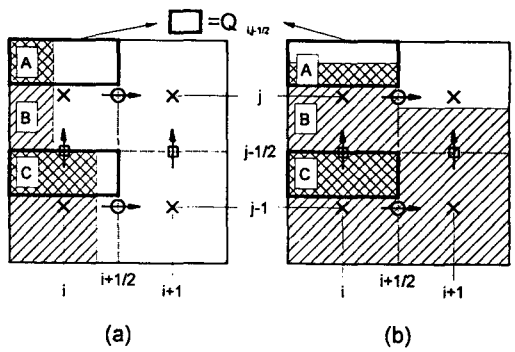

Fig. 4 The mechanism to put the cross-directional upstream effects into the flux. All the hatched regions indicates domain filled with fluid 1.

$$C^C = f^{B+}_{i,j} = a^B_{i,j} Fy(i, j-1/2, Q_{i,j-1/2}, C, V, \theta), \quad (12a)$$

where $a^B_{i,j} = \max[0, sign(Q_{i,j-1/2})]$.

The remained task is to calculate the area of region B, which can be readily accomplished by subtracting the area of region A from the area of region (A+B). The area of region A can be interpreted to be the amount of the volume fraction advected out to the upper cell $(i, j+1)$ from the cell (i, j) due to $Q_{i,j-1/2}$. This quantity can be determined as

$$C^A = f^{B-}_{i,j} = a^B_{i,j} Fy(i, j+1/2, Q_{i,j-1/2}, C, V, \theta). \quad (13)$$

The area of region B becomes

$$C^B = C^{A+B} - C^A = C^n_{i,j} - C^A. \quad (14)$$

Finally, $C^{n+1/2}_{i,j}$ containing the impact of vertical transport from the bottom cell $(i,j-1)$, can be acquired:

$$C^{n+1/2}_{i,j} \approx C^n_{i,j} + \frac{f^{B+}_{i,j} - f^{B-}_{i,j}}{2V_{i,j}}. \quad (15)$$

In this way, $f_{i+1/2,j}$, evaluated by using $C^{n+1/2}_{i,j}$ contains the cross-directional upstream effects.

The above idea can be extended to general situations. Consider all the positive volume fluxes advected into the cell (i, j) from the neighboring cells. The vertical flux of C advected into the cell (i, j) from the upper cell due to a negative volume flux at the top boundary $Q_{i,j+1/2}(<0)$ and the associated flux advected out of the cell (i, j) to the lower cell $(i, j-1)$ can be estimated similarly,

$$f^{T\pm}_{i,j} = a^T_{i,j} Fy(i, j\pm 1/2, Q_{i,j+1/2}, C, V, \theta), \quad (16)$$

where $a^T_{i,j} = \min[0, sign(Q_{i,j+1/2})]$. Likewise, the contributions of the horizontal fluxes advected into the cell (i, j) from the left and right vertical boundaries can be evaluated,

$$f^{L\pm}_{i,j} = a^L_{i,j} Fx(i\mp 1/2, j, Q_{i-1/2,j}, C, V, \theta), \quad (17)$$

$$f^{R\pm}_{i,j} = a^R_{i,j} Fx(i\pm 1/2, j, Q_{i+1/2,j}, C, V, \theta), \quad (18)$$

where $a^L_{i,j} = \max[0, sign(Q_{i-1/2,j})]$ and $a^R_{i,j} = \min[0, sign(Q_{i+1/2,j})]$.

Here, two temporary volume fractions at an intermediate time step *n+1/2* are defined. These contain the effects of vertical and horizontal transports of the volume fraction from the upstream cells, respectively:

$$C^Y_{i,j} = C^n_{i,j} + \frac{f^{B+}_{i,j} - f^{B-}_{i,j} + f^{T+}_{i,j} - f^{T-}_{i,j}}{2V_{i,j}}, \quad (19)$$

$$C^X_{i,j} = C^n_{i,j} + \frac{f^{L+}_{i,j} - f^{L-}_{i,j} + f^{R+}_{i,j} - f^{R-}_{i,j}}{2V_{i,j}}. \quad (20)$$

Now, the horizontal and vertical fluxes of C are determined by using the values $C^X_{i,j}$ and $C^Y_{i,j}$, respectively. Therefore, the present fluxing scheme yields

$$f^*_{i-1/2,j} = Fx(i-1/2, j, Q_{i-1/2,j}, C^Y, V, \theta) \quad (21a)$$

$$f^{*}_{i,j-1/2} = Fy(i, j-1/2, Q_{i,j-1/2}, C^{X}, V, \theta) \quad (21b)$$

It is noted that the scheme of Eq. (21) seems almost the same as that of Eq. (9) of Lafaurie et al. [5]. In fact, the same values of Q and Δt are used. The only difference is that $C^{n}_{i,j}$ is replaced by $C^{X}_{i,j}$ and $C^{Y}_{i,j}$ to incorporate the cross-directional upstream influences.

It is worth pointing out that the procedure of Eqs. (12)-(21) is free from a directional bias. The extension of the present method for the three-dimensional situations is straightforward.

4. Interlink with FCT for Monotonicity

An essential aspect of the advection scheme of Eq. (21) is a judicious blending of the upwind and downwind schemes and the front-sharpening feature is originated from the downwind scheme. The antidiffusive nature of the downwind scheme is useful for interface-capturing, but it leads to a defect that the monotonic solution is not guaranteed. A non-monotone advection scheme can generate unphysical overshoots and/or undershoots. In order to prevent such a deficiency, a cut-off filtering has been executed in calculating the fluxes, such that C should be bounded between 0 and 1. This artificial cut-off may, in turn, result in a local gain or loss of the fluid volume. In the present study, a more reasonable method to realize the monotonicity is explored.

The flux-corrected transport (FCT) is a technique to achieve both monotonicity and accuracy of an advection scheme which are mutually exclusive [7-9]. The basic idea of FCT is the two-step evaluation of the advection terms; a fully-diffusive monotonic solution is acquired and subsequently a higher-order antidiffusive flux is superposed on the diffusive solution to reduce numerical diffusion. Among others, the generalized formulation of FCT by Zalesak [8] has several attractive features. First, the formulation is essentially multi-dimensional, which produces no directional bias. More appealing is the generality of the formulation; monotonicity can be ensured by using combination of any lower-order diffusive scheme and any accurate higher-order advection scheme. The detailed flux correcting procedure of Zalesak will not be reproduced, which can be referred to [8].

It is worth pointing out that, although the cross-directional upstream effects are included, the present advection scheme consists of two basic fluxing schemes, i.e., the diffusive upwind scheme and the downwind scheme of antidiffusive nature. It is then advantageous to treat the flux given by the upwind scheme as the diffusive flux, and to define the flux given by the downwind scheme as the higher-order anti-diffusive flux, i.e.,

$$f^{L}_{i-1/2,j} = f^{u}_{i-1/2,j} = Q_{i-1/2,j} C_{i-1/2-p/2,j}, \quad (22a)$$

$$f^{L}_{i,j-1/2} = f^{u}_{i,j-1/2} = Q_{i,j-1/2} C_{i,j-1/2-q/2}, \quad (22b)$$

$$f^{H}_{i-1/2,j} = f^{*}_{i-1/2,j}, \quad (23a)$$

$$f^{H}_{i,j-1/2} = f^{*}_{i,j-1/2}. \quad (23b)$$

By using these fluxes, the Zalesak's generalized FCT procedure can be applied as follows.

(i) Compute $f^{L}_{i-1/2,j}$, $f^{L}_{i,j-1/2}$ and $f^{H}_{i-1/2,j}$, $f^{H}_{i,j-1/2}$.

(ii) Compute the updated lower-order transported and diffused solution,

$$C^{td(k+1)}_{i,j} = C^{n+1(k)}_{i,j}. \quad (24)$$

(iii) Define the antidiffusive fluxes,

$$f^{ad(k+1)}_{i-1/2,j} = (1-\beta^{(k)}_{i-1/2,j}) f^{ad(k)}_{i-1/2,j}, \quad (25a)$$

$$f^{ad(k+1)}_{i,j-1/2} = (1-\beta^{(k)}_{i,j-1/2}) f^{ad(k)}_{i,j-1/2}. \quad (25b)$$

(iv) Limit the antidiffusive fluxes,

$$f^{c(k+1)}_{i-1/2,j} = \beta^{(k+1)}_{i-1/2,j} f^{ad(k+1)}_{i-1/2,j}, \quad (26a)$$

$$f^{ad(k+1)}_{i,j-1/2} = \beta^{(k+1)}_{i,j-1/2} f^{ad(k+1)}_{i,j-1/2}. \quad (26b)$$

(v) Apply the limited antidiffusive fluxes to obtain

new values, $C_{i,j}^{n+1}$,

$$C_{i,j}^{n+1(k+1)} = C_{i,j}^{td(k+1)} + \frac{f_{i-1/2,j}^{c(k+1)} - f_{i+1/2,j}^{c(k+1)} + f_{i,j-1/2}^{c(k+1)} - f_{i,j+1/2}^{c(k+1)}}{V_{i,j}}. \quad (27)$$

In the above, k denotes the iteration level. The Zalesak's flux limiting of Eqs. (24)-(27) was originally a one-through-step method biased to the strategy of guaranteeing a monotone solution [8]. Under the present situation $O(f^L) \sim O(f^{ad})$ near interface, one-through-step evaluation of fluxes does not provide sufficient antidiffusion to be applicable without violating monotonicity; rather, it gives only a minimal antidiffusion. In order to satisfy both the constraints of surface-sharpening and monotonicity, an iterative routine is designed as shown in Eqs. (24)-(27). The values at zero-iteration step (initial guess) are given as follows:

$$C_{i,j}^{n+1(0)} = C_{i,j}^{n} + \frac{f_{i-1/2,j}^{L} - f_{i+1/2,j}^{L} + f_{i,j-1/2}^{L} - f_{i,j+1/2}^{L}}{V_{i,j}}, \quad (28)$$

$$f_{i-1/2,j}^{ad(0)} = f_{i-1/2,j}^{H} - f_{i-1/2,j}^{L}, \quad (29a)$$

$$f_{i,j-1/2}^{ad(0)} = f_{i,j-1/2}^{H} - f_{i,j-1/2}^{L}, \quad (29b)$$

$$\beta_{i-1/2,j}^{(0)} = \beta_{i-1/2,j}^{(0)} = 0. \quad (30)$$

Iteration is performed until the relative variations between two successive iteration steps fall below a prescribed value. It is noted that this iteration does not create new maxima or minima since the antidiffusive fluxes are limited to ensure the monotonic solution at each iteration step. Only a right amount of the antidiffusive flux, which does not produce new extrema but was not included in the previous iteration step, is considered in the new iteration step. This method becomes identical to the original FCT of Zalesak if only one iteration is conducted.

5. Results of Verification Tests

Two simple test problems which were considered by Lafaurie et al. [5] are reproduced to reveal the interface-capturing feature of the present advection scheme.

First, consider a 10×10 square domain of cells on a grid system with a uniform spacing $\Delta x = \Delta y = 1$. This block is transported diagonally via a uniform velocity field $(u,v)=(1,1)$ until $t=50$. Numerical experiments were conducted by applying the present advection scheme and the scheme of Lafaurie et al. [5] with the same condition $\theta^c = 1.05$. The results are illustrated in Fig. 5 by depicting contour plots for the values of volume fraction, C=0.05, 0.4, 0.6, 0.95.

It is discernible that the previous method of Eq. (9) produces noticeable distortions near the corner regions as illustrated in Fig. 3. In contrast, the present advection scheme yields an improved feature of maintaining the shape. This is indicative of the fact the distortions near the corner regions are mainly responsible for the aforementioned one-dimensional representation of the fluxes. The present advection scheme suppresses much of this local numerical error by incorporating the cross-directional upstream effects into the fluxes.

An essential task in assessing the accuracy of an advection scheme for volume fraction is to measure global change of interface in which both of diffusion and distortion of interface are included. In an effort to quantify global change of interface, a parameter to represent an error relative to the exact solution is defined as

$$E = \frac{\sum_i \sum_j |C_{i,j}^{e} - C_{i,j}^{ns}|}{\sum_i \sum_j C_{i,j}^{e}}, \quad (31)$$

where the superscripts e and ns denote the exact solution and the numerical solution, respectively. The values of E for the corresponding cases are also given in Fig. 5. It is clear that the present advection scheme gives much smaller values of

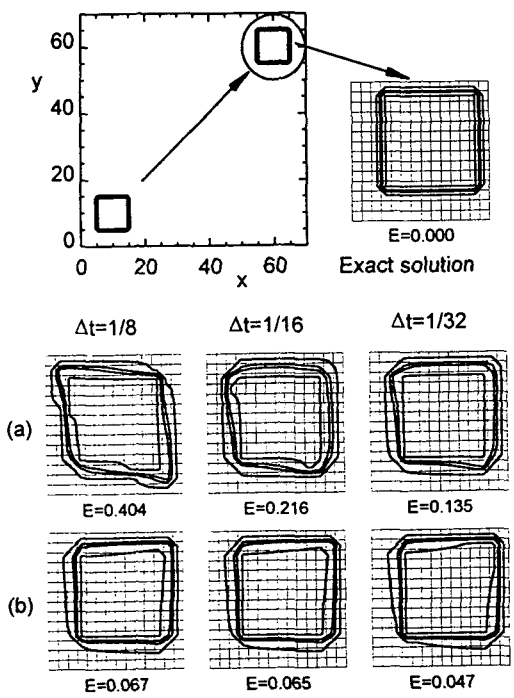

Fig. 5 Results of pure translation of a square domain at t=50: (a) the previous scheme of Eq. (9); (b) the present advection scheme. The value of E defined in Eq. (31) is given in the lower part of each frame.

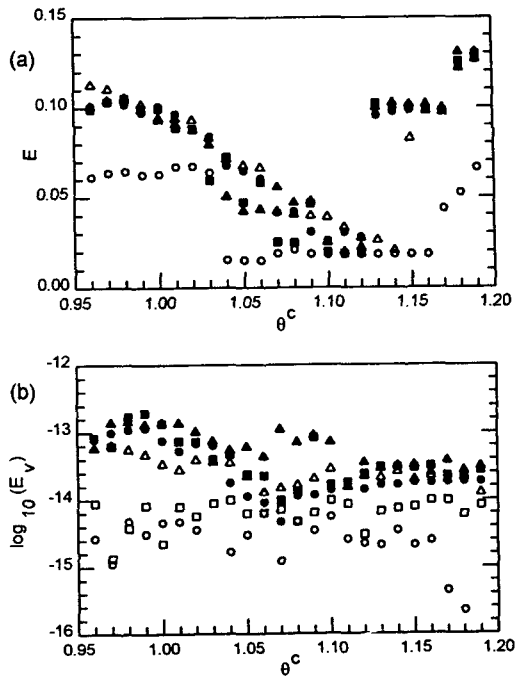

Fig. 6 Numerical errors of the present advection scheme for the problem in Fig. 5: (a) E; (b) E_v. Errors are estimated at time t=50 by using different time increment ○, Δt=1/2; □, Δt=1/4; △, Δt=1/8; ●, Δt=1/16; ■, Δt =1/32; ▲, Δt=1/64.

E in comparison with the scheme of Eq. (9). In view of both local and global shape changes, the present advection scheme displays improved features of interface transport.

Additional important finding in Fig. 5 is that numerical error of the present scheme does not vary significantly with time step Δt. It is worth pointing out that the accuracy of conventional VOF methods [4,5] is very sensitive to time step. As shown in Fig. 5, even for a time step satisfying CFL condition, numerical error of the scheme of Eq. (9) becomes more conspicuous as Δt increases (see both the shape and the value of E). Owing to the second order accuracy in time, the present advection scheme gives a better behavior with variation of Δt.

Numerical tests were also performed by varying the critical angle θ^c and Δt. The results are summarized in Fig. 6. It is seen that a principal parameter to determine numerical error is θ^c rather than Δt. It is confirmed that the numerical accuracy of the present advection scheme is less sensitive to Δt. Fig. 6(a) suggests the optimal value of the critical angle $1.07 \leq \theta^c \leq 1.11$. Here, it should be noted that this estimation is made from a test of transport of a square block in uniform velocity field. The optimum value of θ^c may be dependent on flow condition and interface shape. A subsequent numerical experiments are needed for finding the optimum value of θ^c under more general flow situations.

An interesting point in Fig. 3 is that E for Δt=1/2 is smaller than those of other cases. This is attributable to the fact that the present scheme was particularly designed to give an improved solution for the problem of rectangular domain propagation under a two-dimensional uniform flow field. It is noted that, for this test problem with $\Delta x = \Delta y = u = v = 1$, Δt is identical to the CFL number, $Co = u\Delta t/\Delta x$. Actually, when Δt=1, the present scheme results in a good solution which is in agreement with the exact solution within machine accuracy. This is in line with the fact that the previous fluxing schemes [4,5] also provides an accurate prediction of one-dimensional interface propagation under the same condition $Co = 1$. Therefore, for this test problem, E decreases as Δt approaches to the CFL value, i.e., Δt=1. A point worth being stressed here is the favorable aspect of the present advection scheme that, for relatively small values of Δt, E is insensitive to Δt.

Another issue in discussing advection scheme for volume fraction is conservation of total volume. Fig. 6(b) exhibits the error of volume conservation defined as

$$E_v = \frac{\sum_i \sum_j C^e_{i,j} - \sum_i \sum_j C^{ns}_{i,j}}{\sum_i \sum_j C^e_{i,j}}. \qquad (32)$$

The present advection scheme is based on the conservative formulation on a finite volume mesh and the monotonicity is guaranteed by adopting FCT procedure without any artificial cut-off. Naturally, the total volume conservation is satisfied within the machine accuracy. The errors depicted in Fig. 6(b) can be interpreted as accumulation of round-off errors.

The second test problem is the rotation of a 30×10 rectangular domain, for which the conventional advection schemes gave poor results (see e.g., Fig. 7 in [5]). The pronounced effect of rotation generated a large amount of flotsam on large lattices, or spikes were created on the flat

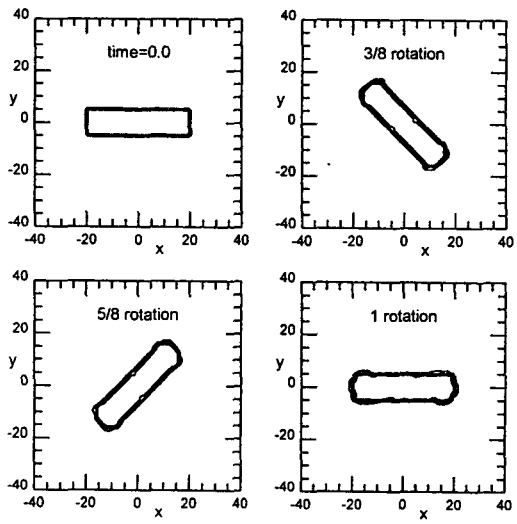

Fig. 7 Results of the rotation of a rectangle.

surfaces of the rectangle. As seen in Fig. 7, the present advection scheme gives better prediction of interface motion; there is no flotsam and deformation of the rectangular shape is much suppressed in comparison to the results in [5].

Finally, the present numerical model is tested for a benchmark flow configuration. In many respects of VOF, the solver to the Navier-Stokes equations constitutes a separate part, which can be pursed independently of the interface capturing described in the previous chapters. For this test, a numerical model based on SIMPLE [10] was used, which was coupled with the calculation routine for C via the density. The broken dam problem in Hirt and Nicholas [4] is reproduced; the water column of 1 units wide and 2 unit high is allowed to flow out along a dry horizontal floor by removing dam at t=0. The gravity vector g is downward. The position of the leading edge of the water vs time is depicted in Fig. 8. The present numerical prediction shows a good agreement with the experimental data [4].

6. Conclusion

An advection scheme based on the VOF is

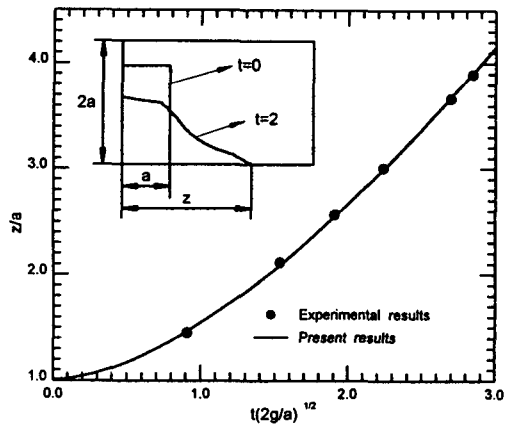

Fig. 8 Comparison of calculated results with experimental data for the broken dam problem.

developed as a means to describe the interface between two immiscible fluids. The key elements of the present scheme are (1) to achieve the second-order time accuracy by taking into account the cross-directional upstream effects, and (2) to guarantee the monotonicity by interlinking it with the FCT technique. Verification tests revealed that the present scheme provides an improved prediction of interface motion in comparison to the prior versions [4-5].

Acknowledgement

Appreciation is extended to the referees who provided valuable comments and suggestions. This research was supported in part by a grant from the ISAS COE Program of the Ministry of Education, Science, Sports and Culture, Japan. Part of this work was performed under the support of SERI, which is to be appreciated.

References

[1] Harlow, F. and Welch, J. E., "Numerical Calculation of Time-Dependent Viscous Incompressible Flow of Fluid with Free Surface," *Phys. Fluids* **9** (1965), p.2182.

[2] Tome, M. F. and McKee, S., "GENSMAC: A Computational Marker and Cell Method for Free Surface Flows in General Domain," *J. Comp. Phys.* **110** (1994), p.171.

[3] Monagan, J. J., "Simulating Free Surface Flows with SPH," *J. Comp. Phys.* **110** (1994), p.399.

[4] Hirt, C. W. and Nicholas, B. D., "Volume of Fluid (VOF) Method for the Dynamics of Free Boundaries," *J. Comp. Phys.* **39** (1981). p.201.

[5] Lafaurie, B. et al., "Modeling Merging and Fragmentation in Multiphase Flows with SUFFER," *J. Comp. Phys.*, **113** (1994), p.134.

[6] Thomas, T. G. et al., "Free Surface Simulations Using a Conservative 3D Code," *J. Comp. Phys.* **116** (1995), p.52.

[7] Oran, E. S. and Boris, J. P., *Numerical Simulation of Reacting Flows*, Elsevier, New York (1987).

[8] Zalesak, S. T., "Fully Multi-Dimensional Flux-Corrected Transport Algorithms for Fluids," *J. Comp. Phys.*, **31** (1979), p.335.

[9] Boris, J. P. et al., "LCPFCT - Flux-Corrected Transport for Generalized Continuity Equations," *NRL Memorandom Report*, Naval Research Laboratory, Washington DC (1987).

[10] Patankar, S. V., *Numerical Heat Transfer and Fluid Flows*, McGraw-Hill, New York (1980).